ORNL/FEDC-84/1
Dist. Category UC-20 c,d

Fusion Energy Division

ORNL/FEDC--84/1

DE85 004386

PLASMA PERFORMANCE OF TFCX AND JET WITH SAWTOOTHING

L. M. Hively
General Electric Company/Fusion Engineering Design Center

D. R. Mikkelsen
Princeton Plasma Physics Laboratory

NOTICE This document contains information of a preliminary nature. It is subject to revision or correction and therefore does not represent a final report.

Date Published - November 1984

Prepared by the
OAK RIDGE NATIONAL LABORATORY
Oak Ridge, Tennessee 37831
operated by
MARTIN MARIETTA ENERGY SYSTEMS, INC.
for the
U.S. DEPARTMENT OF ENERGY
Under Contract No. DE-AC05-84OR21400

CONTENTS

ABSTRACT

The plasma performance is assessed for two tokamak reactor experiments, the Tokamak Fusion Core Experiment (TFCX) and the Joint European Torus (JET). Both machines appear ignitable for a reasonable range of transport assumptions.

1. INTRODUCTION

In this report we assess performance for the Tokamak Fusion Core Experiment (TFCX) and the Joint European Torus (JET). We use both the Plasma OPeration CONtour (POPCON) analysis and dynamic startup simulations using the WHIST transport code.[1] For a given set of transport assumptions and machine parameters, we find there is a significant operating regime in density-temperature space. The performance and auxiliary heating requirements are altered substantially by variations in the transport assumptions, so flexibility and robustness in the performance have also been assessed.

2. PHYSICS MODEL

Plasma simulations are based on the work of Houlberg et al.[1] Previous work and details of the model are described in ref. 2; a summary of the model follows. The noncircular plasma equilibrium (consistent with particle, temperature, and current profiles) is treated using the Lao moments method.[2,3] By using flux-coordinate labeling, the noncircular (two-dimensional) transport problem is reduced to one dimension. Evolution of the various profiles is followed in flux coordinates using conservation of particles (five ion species plus electrons), energy (ions and electrons), and poloidal flux. The model includes simple edge/divertor physics and fixed impurities (five species) with coronal radiation losses using the model of Post et al.[4] Ohmic heating and local, instantaneous alpha particle deposition are supplemented by Gaussian heating $\{\sim\exp[-(r/r_0)^2]\}$, which is strongly peaked in the local minor radius (r) similar to ion cyclotron resonance heating (ICRH). The rf-like power is split between ions (75%) and electrons (25%) with $r_0 = 0.8$ m. Fueling of the deuterium-tritium (D-T) plasma is by gas puffing with a 95% recycling fraction.

Sawtoothing is an important aspect of these simulations that occurs when the on-axis safety factor q(0) drops below one. The strong central heating lowers the plasma resistivity and restricts the current channel. The centrally peaked current density rises, lowering q(0) below unity and initiating the sawtooth instability. The density, temperature, and current profiles are flattened by turbulence inside the sawtoothing region, which is consistent with conservation of particles, energy, and helical flux. Further poloidal flux diffusion allows this cycle to periodically repeat with an expected period of 400 ms in TFCX[5] as compared with an energy confinement time >1 s. The resulting central turbulence typically extends to three-fourths of the minor plasma radius; this is consistent with experiments.[6] The profile for q is flat for $r/a \leq 0.75$, rising abruptly to q(a) for $r/a > 0.75$. Consequently, plasma losses are dominated by confinement in the outer plasma, where gradients are large and the typical temperature is low, resulting in a current relaxation time ∿30 s. Plasma parameters are time averaged over each sawtooth period to obtain the quasi-static POPCON performance. Without sawtoothing, $q(0) \lesssim 0.4$ is typical with a well-confined core plasma, lower gradients, and higher temperature that result in a resistive decay time ∿250 s. The performance with sawtoothing is much poorer than without sawtoothing.

The transport assumptions include neoclassical losses that are twice those given by Hinton and Hazeltine.[7] The Hastie-Hitchon model[8] is used for the thermal ion conduction loss by toroidal field ripple, assuming an edge ripple of 1.5% and 16 toroidal field (TF) coils. Ripple losses increase as the magnetic axis shifts outward during evolution of the magnetohydrodynamic (MHD) equilibrium. Anomalous electron energy confinement and particle diffusion ($D = \chi/5$) are a version of neo-Alcator (NA) scaling,[9]

$$\chi_{NA}\ (\mathrm{cm^2/s}) = \left[\frac{1.5 \times 10^{17}}{n_e\ (\mathrm{cm^{-3}})}\right]\left[\frac{r}{43\ (\mathrm{cm})}\right]\left[\frac{250\ (\mathrm{cm})}{R_o}\right]^2 , \qquad (1)$$

and a modified form of ref. 10 (GMS),

$$\chi_{GMS}\ (\mathrm{cm^2/s}) = 65[1 + 4(r/a)^2]\ \frac{a\ (\mathrm{cm})\ \sqrt{\kappa}}{I\ (\mathrm{MA})} . \qquad (2)$$

Here, n_e is the local electron density, I is the plasma current, and r is the local minor radius on the midplane. A finite-beta enhancement of the GMS scaling is included:

$$f(\beta) = 0.384\ \exp[(\beta/\beta_c)^2]\ , \tag{3a}$$

$$\beta_c = \left[\frac{a}{5R_0 q(a)}\right]\left(\frac{1+\kappa^2}{2}\right)\ , \tag{3b}$$

so that $f(\beta = \beta_c) \sim 1$, with β_c generalized from ref. 11 for a non-circular plasma. An anomalous electron conduction coefficient is taken as

$$\chi_e = \chi_{NA} + 0.72\chi_{GMS} \times f(\beta) \tag{4}$$

to model the ohmic confinement (χ_{NA}) together with the high-beta, auxiliary heating scaling $[0.7\chi_{GMS} \times f(\beta)]$. The anomalous particle diffusion coefficient is taken as $D = \chi_{Ee}/5$.

3. RESULTS FOR TFCX

3.1 PLASMA PERFORMANCE

The nominal copper TFCX design[12] was chosen as a representative example having the following parameters:

Parameter	Value
Major radius, R_0 (m)	3.25
Minor radius, a (m)	1.30
Elongation, κ	1.6
Triangularity, δ	0.3
On-axis field, B_0 (T)	4.00
Safety factor, q(a)	2.4

Other TFCX devices have similar performance parameters.

Using the method of ref. 1, Fig. 1 shows the Plasma OPeration CONtours (POPCONs) assuming neo-Alcator confinement [Eq. (1)] with sawtoothing. There is 10% hydrogen to simulate dilution of the fusion source during ICRH H-minority heating. The auxiliary power at quasi-static equilibrium (P_{aux}^{eq}) is required to maintain the operating point in density (n_e) and temperature (T) space [Fig. 1(a)] against confinement losses. Ignition corresponds to the contour of zero auxiliary power ($P_{aux}^{eq} = 0$) in Fig. 1(a). The minimum ignition density lies at $n_e = 7 \times 10^{13}$ cm^{-3} and T = 16 keV, corresponding to a fusion power P_{fus} of 200 MW [Fig. 1(b)], a toroidal beta β_T of 7% [Fig. 1(c)], and a poloidal beta β_p of 0.7 [Fig. 1(d)]. Large auxiliary powers [Fig. 1(a)] at low density and high temperature are needed to overcome thermal ion losses due to TF ripple. Increasing auxiliary power allows this ripple loss to be surmounted as fusion power becomes dominant. An ignition margin M of 1.5 is denoted by the dotted contour in Fig. 1(a), where

$$M = \frac{\text{(fusion power from alphas)}}{\text{(power lost) - (ohmic heating power)}} \equiv \frac{P_\alpha}{P_L - P_{OH}} ,$$

and indicates the depth of the superignited domain. Ignition is the same as M = 1. The performance for neo-Alcator scaling is optimistic, making a large extrapolation from ohmically heated experiments.

Figure 2 shows POPCONs, assuming GMS scaling [Eq. (2)] with sawtoothing and 10% hydrogen. The minimum ignition density lies at $n_e = 7 \times 10^{13}$ cm^{-3} with 14 keV $\leq$ T $\leq$ 18 keV [Fig. 2(a)], corresponding to 200 MW $\leq P_{fus} \leq$ 300 MW [Fig. 2(b)], 6% $\leq \beta_T \leq$ 8% [Fig. 2(c)], and $0.6 \leq \beta_p \leq 0.7$ [Fig. 2(d)]. Since GMS scaling is more optimistic than neo-Alcator for auxiliary heating, lower powers are necessary to overcome the thermal ion TF ripple losses. At low β_T values, the shift in the magnetic axis is small, requiring less plasma current than at high β_T with fixed q(a) = 2.4. There is a corresponding reduction in confinement since $\chi_{GMS} \sim 1/I$ [Eq. (2)], thus requiring somewhat larger auxiliary powers [Fig. 2(a)] to maintain operation at high density and low temperature. There is a saddle point in the intermediate region

ORNL–DWG 84-3083 FED

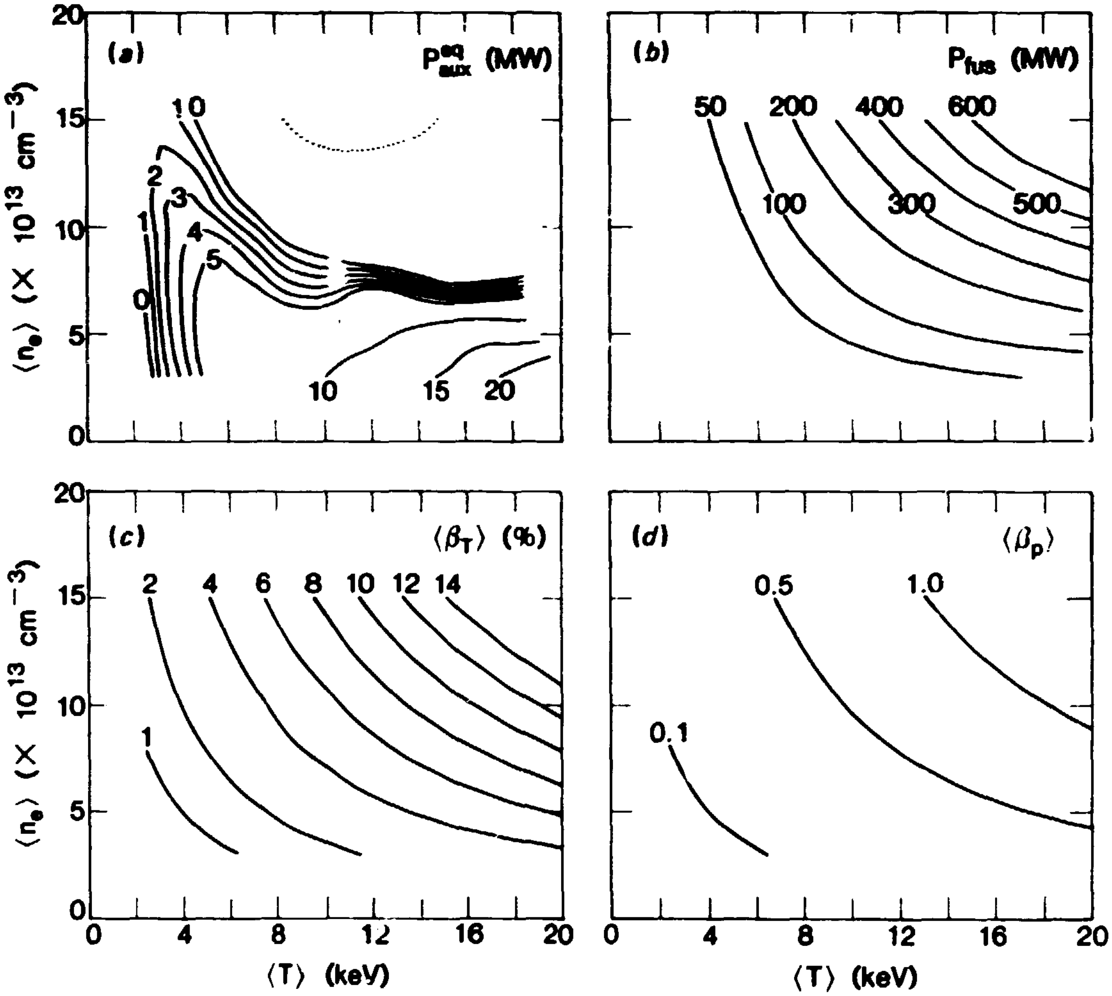

Fig. 1. Plasma OPeration CONtours (POPCONs) for (a) auxiliary power, (b) fusion power, (c) toroidal beta, and (d) poloidal beta, assuming neo-Alcator confinement.

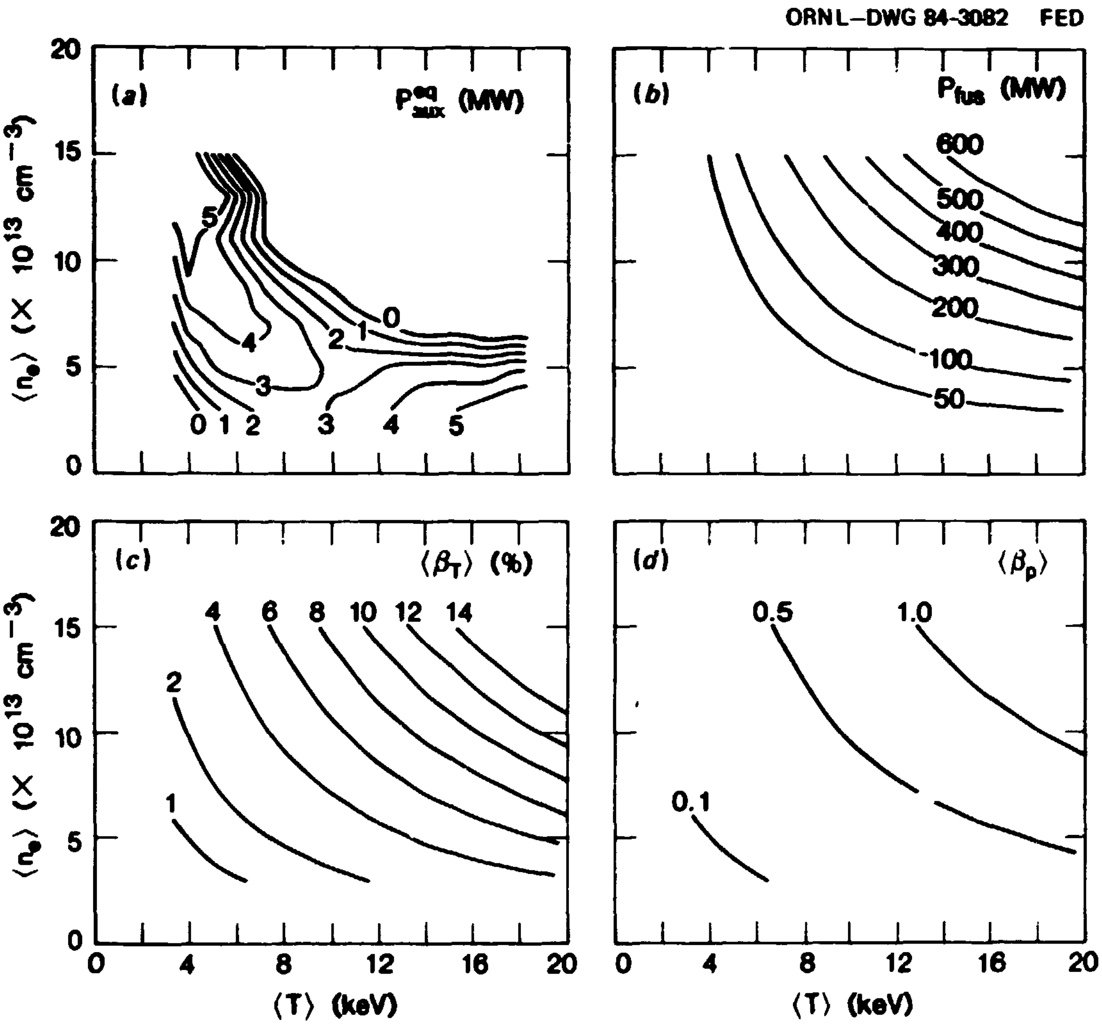

Fig. 2. POPCONs assuming GMS scaling.

[Fig. 2(a)] near $n_e = 4 \times 10^{13}$ cm^{-3} and T = 10 keV. The performance for GMS scaling alone is also optimistic because ohmic losses (i.e., neo-Alcator scaling) are not included.

Figure 3 shows POPCONs assuming a combination of GMS scaling with a soft-beta enhancement [Eq. (4)], sawtoothing, and neo-Alcator scaling of the form:

$$\chi_{NA}\ (cm^2/s) = \left[\frac{1.5 \times 10^{17}}{n_e\ (cm^{-3})}\right]\left[\frac{a\sqrt{\kappa}}{83\ (cm)}\right]\left[\frac{250\ (cm)}{R_o}\right]^2 . \qquad (5)$$

The minimum ignition density lies at $n_e = 7 \times 10^{13}$ with T = 12 keV [Fig. 3(a)], corresponding to P_{fus} = 150 MW [Fig. 3(b)], β_T = 5.5% [Fig. 3(c)], and β_p = 0.5 [Fig. 3(d)]. The finite-beta enhancement to χ_{Ee} limits the ignition region [Fig. 3(a)] to $P_{fus} < 300$ MW [Fig. 3(b)], $\beta_T < 8\%$ [Fig. 3(c)], and $\beta_p < 0.7$ [Fig. 3(d)]. These results are optimistic at low temperature because impurity radiation losses are not included.

Figure 4 illustrates POPCON results assuming a combination of neo-Alcator and β_T-enhanced GMS scalings [Eqs. (4) and (5)] with sawtoothing and 1.5% oxygen. There is no ignition region. The minimum power near ignition is <2 MW at $n_e = 0.9 \times 10^{14}$ cm^{-3} and T = 10 keV [Fig. 4(a)], corresponding to P_{fus} = 150 MW [Fig. 4(b)], β_T = 5% [Fig. 4(c)], and β_p = 0.5 [Fig. 4(d)]. The large auxiliary powers required to operate at low temperature and high density are due to oxygen impurity radiation loss. This result is probably pessimistic because experiments can obtain a constant impurity density with increasing n_e (rather than a constant impurity fraction).

Figure 5 displays POPCON results with transport scaling given by Eqs. (4) and (5) with sawtoothing and a constant oxygen density of 6 × 10^{11} cm^{-3}. The minimum ignition point lies at $n_e = 10^{14}$ cm^{-3} and T = 9 keV, corresponding to P_{fus} = 150 MW [Fig. 4(b)], β_T = 5% [Fig. 4(c)], and β_p = 0.5 [Fig. 4(d)]. The dotted contour in Fig. 4(a) corresponds to an ignition margin M of 1.05. As before, large auxiliary powers [Fig. 4(a)] at low n_e and high T are needed to overcome thermal ion losses due to TF

ORNL–DWG 84-2939 FED

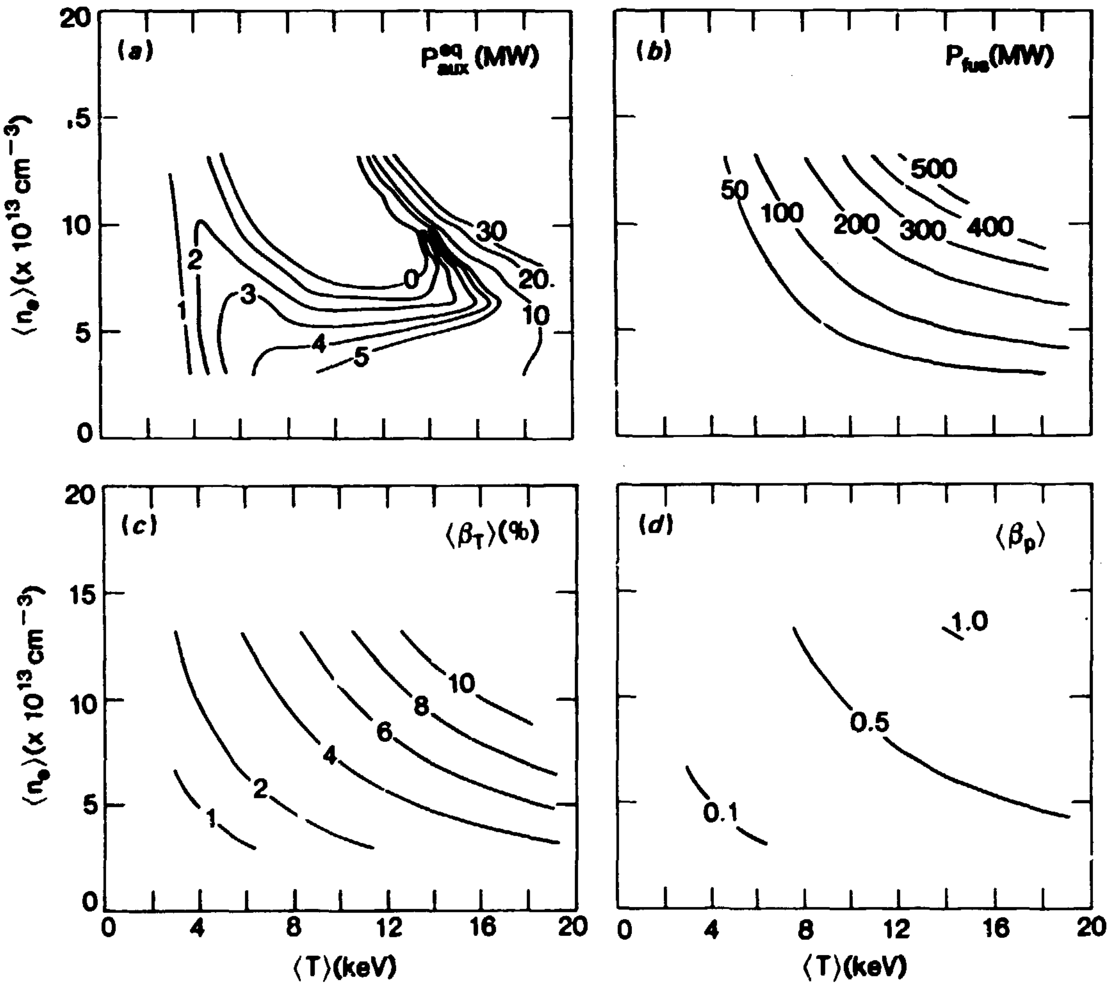

Fig. 3. POPCONs for neo-Alcator scaling and GMS scaling with a soft-beta enhancement.

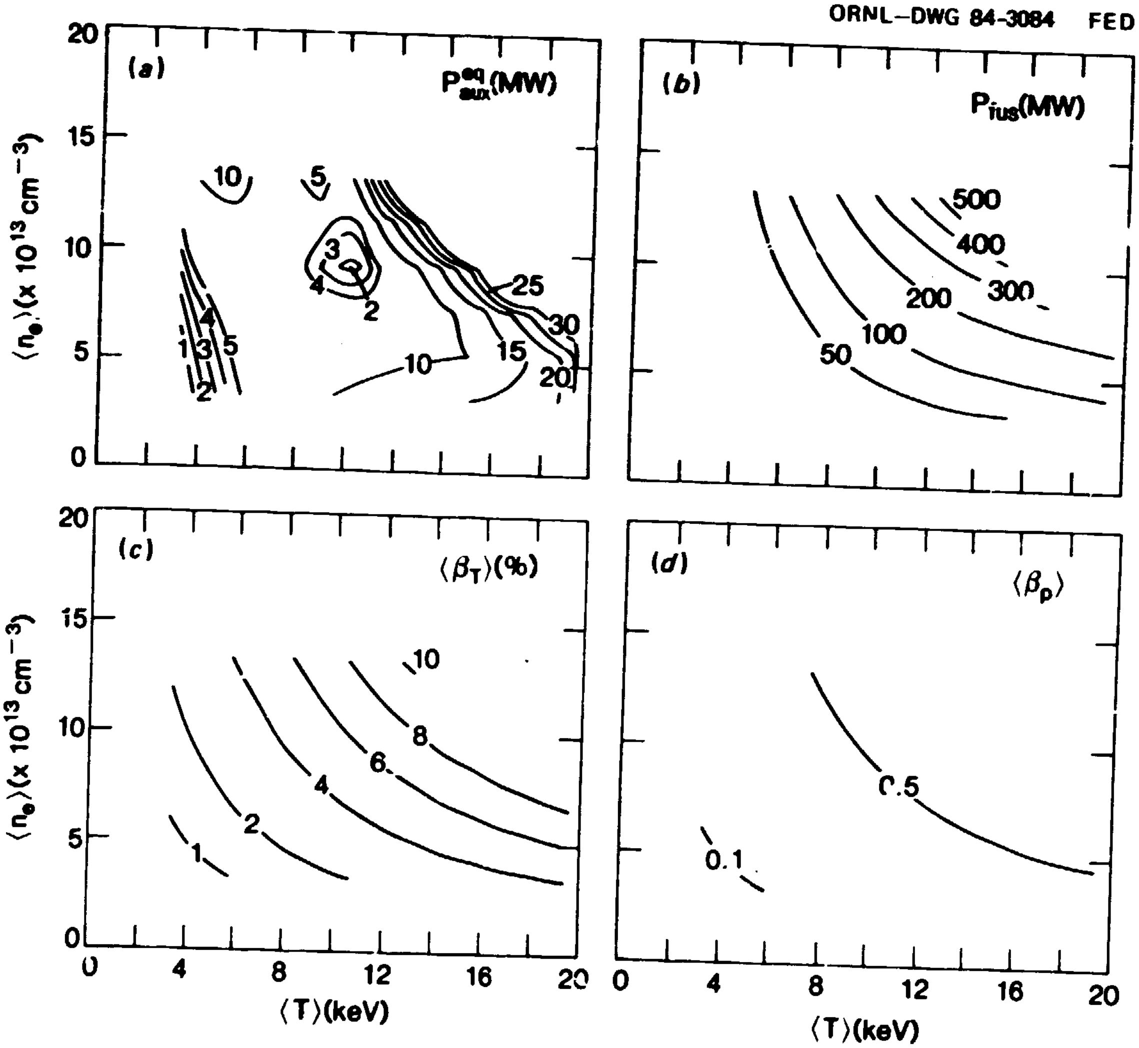

Fig. 4. POPCONs assuming $\chi_{NA} + 0.72\chi_{GMS} \times f(\beta/\beta_c)$ with 1.5% oxygen impurity.

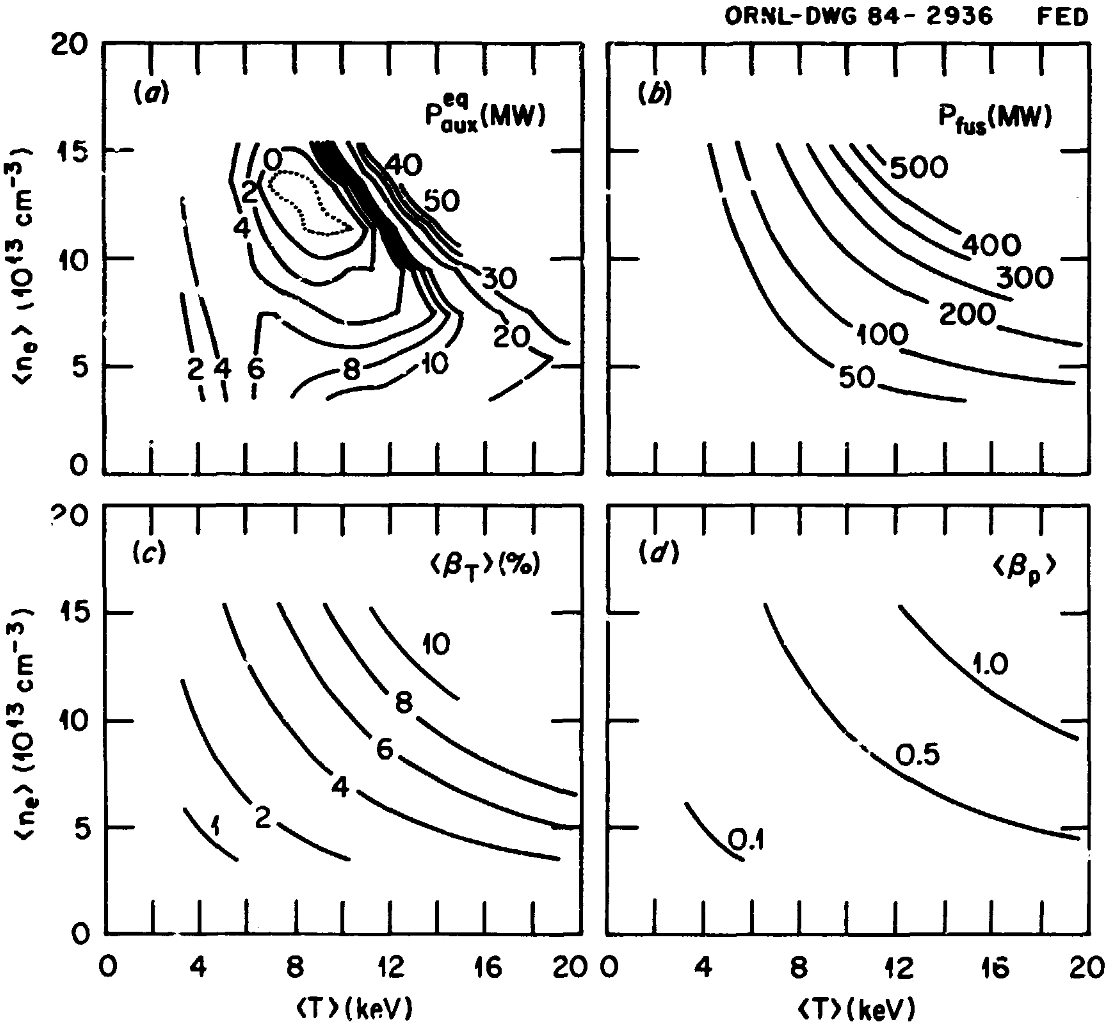

Fig. 5. POPCONs assuming $\chi_{NA} \div 0.72\chi_{GMS} \times f(\beta/\beta_c)$ and n_{ox} = 6×10^{11} cm^{-3}.

ripple. High powers at low T and high n_e are required to offset impurity radiation losses. The finite-beta enhancement to χ_{Ee} limits the ignition region [Fig. 5(a)] to $P_{fus} < 300$ MW [Fig. 5(b)], $\beta_T < 7.5\%$ [Fig. 5(c)], and $\beta_p < 0.7$ [Fig. 5(d)]. There is a shallow saddle point in Fig. 5(a) ($P_{aux}^{eq} \sim 5$ MW); an auxiliary power of >5 MW would barely surmount this saddle point, corresponding to an infinite startup time. Applying 10 MW of ICRH-like auxiliary power results in a 10-s startup time from ohmic state to the minimum ignition point. There is a ±10 to 15% variation in the power to the divertor and ion source rate to the plasma due to sawtoothing. A maximum auxiliary heating power of ≤ 25 MW therefore appears more than adequate to start up and maintain the plasma over a wide range of operation points and confinement scaling.

Figure 6 shows the performance of TFCX when q(a) is increased from 2.4 to 2.6. Ignition lies inside the small closed contour [Fig. 6(a)] centered at T = 8 keV and $n_e = 1.3 \times 10^{14}$ cm^{-3}, corresponding to $P_{fus} \sim 200$ MW [Fig. 6(b)], $\beta_T \sim 5.5\%$ [Fig. 6(c)], and $\beta_p \sim 0.6$ [Fig. 6(d)]. Ignition occurs for $\beta_T \lesssim 6\%$, which is somewhat lower than the previous case because β_c is inversely proportional to q(a) from Eq. (3b).

Figure 7 illustrates the performance when the toroidal field is reduced from 4 T to 3.5 T. There is a plateau in the auxiliary power ($P_{aux}^{eq} \sim 7$ MW) centered at T = 7 keV and $n_e = 10^{14}$ cm^{-3} [Fig. 7(a)]. There is no ignition region.

Figure 8 illustrates the improved performance if the soft-beta limit β_c is raised by 33% consistent with ref. 13 for a TFCX plasma; that is, if the right side of Eq. (3b) is multiplied by 1.33. The ignition region is expanded [Fig. 8(a)] in comparison to Fig. 5 with a maximum ignition margin M of 1.25 as shown by the dotted contours in Fig. 8(a). The minimum in the ignition contour lies at T = 13 keV and $n_e = 8.5 \times 10^{13}$ cm^{-3}, corresponding to $P_{fus} = 200$ MW [Fig. 8(b)], $\beta_T = 7\%$ [Fig. 8(c)], and $\beta_p = 0.6$ [Fig. 8(d)]. The auxiliary power to reach ignition is unchanged from Fig. 5.

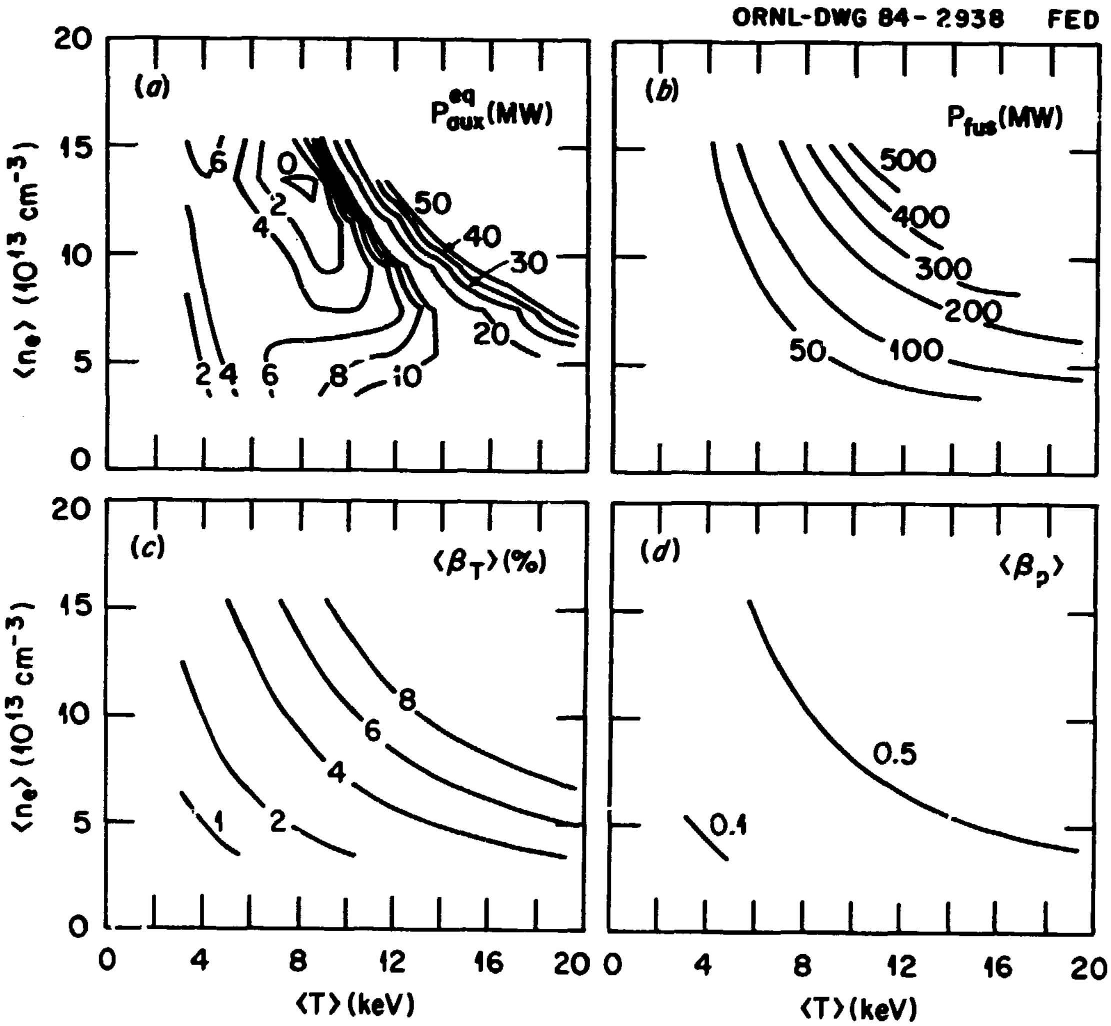

Fig. 6. POPCONs assuming $\chi_{NA} + 0.72\chi_{GMS} \times f(\beta/\beta_c)$ and n_{ox} = 6×10^{11} cm^{-3} with q(a) = 2.6.

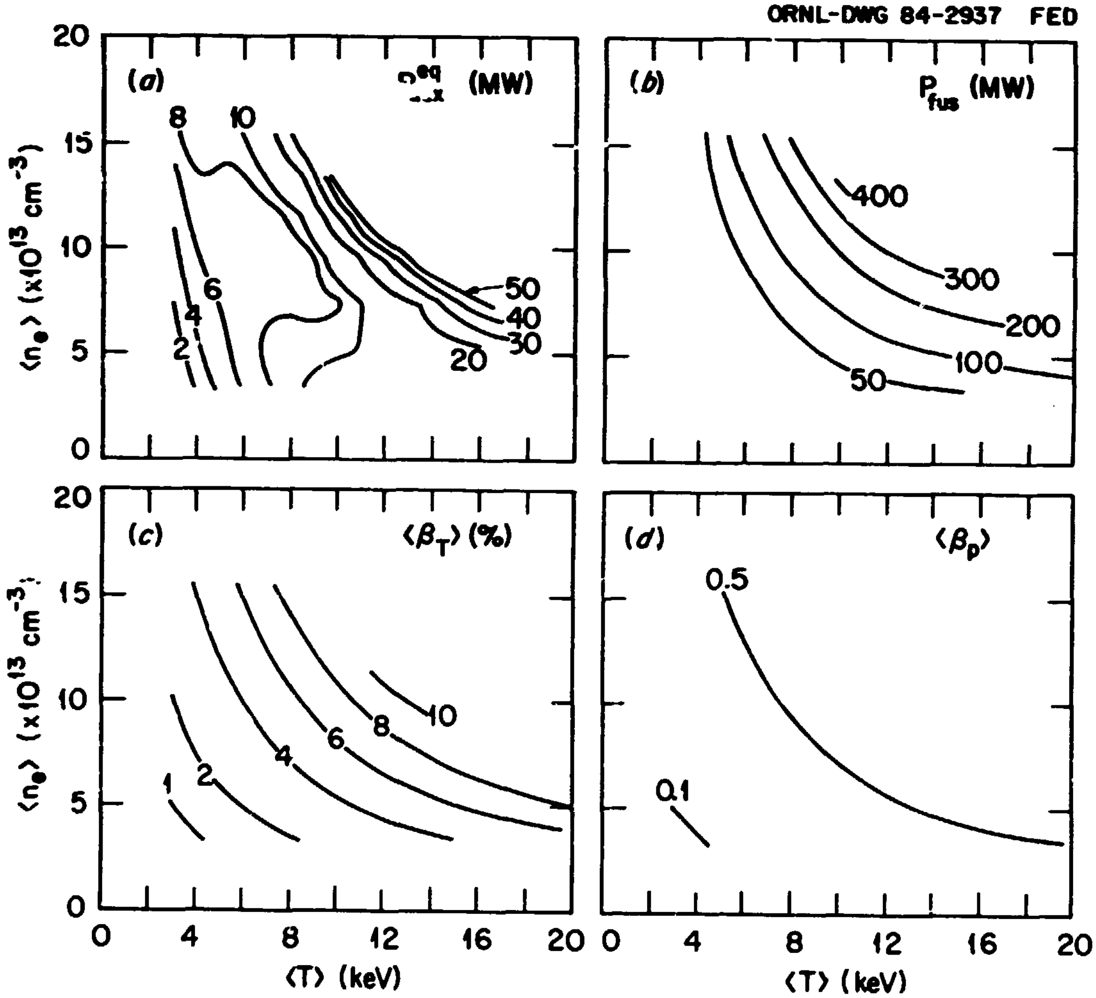

Fig. 7. POPCONs assuming $\chi_{NA} + 0.72\chi_{GMS} \times f(\beta/\beta_c)$ and $n_{ox} = 6 \times 10^{11}\ cm^{-3}$ with $B_T = 3.5$ T.

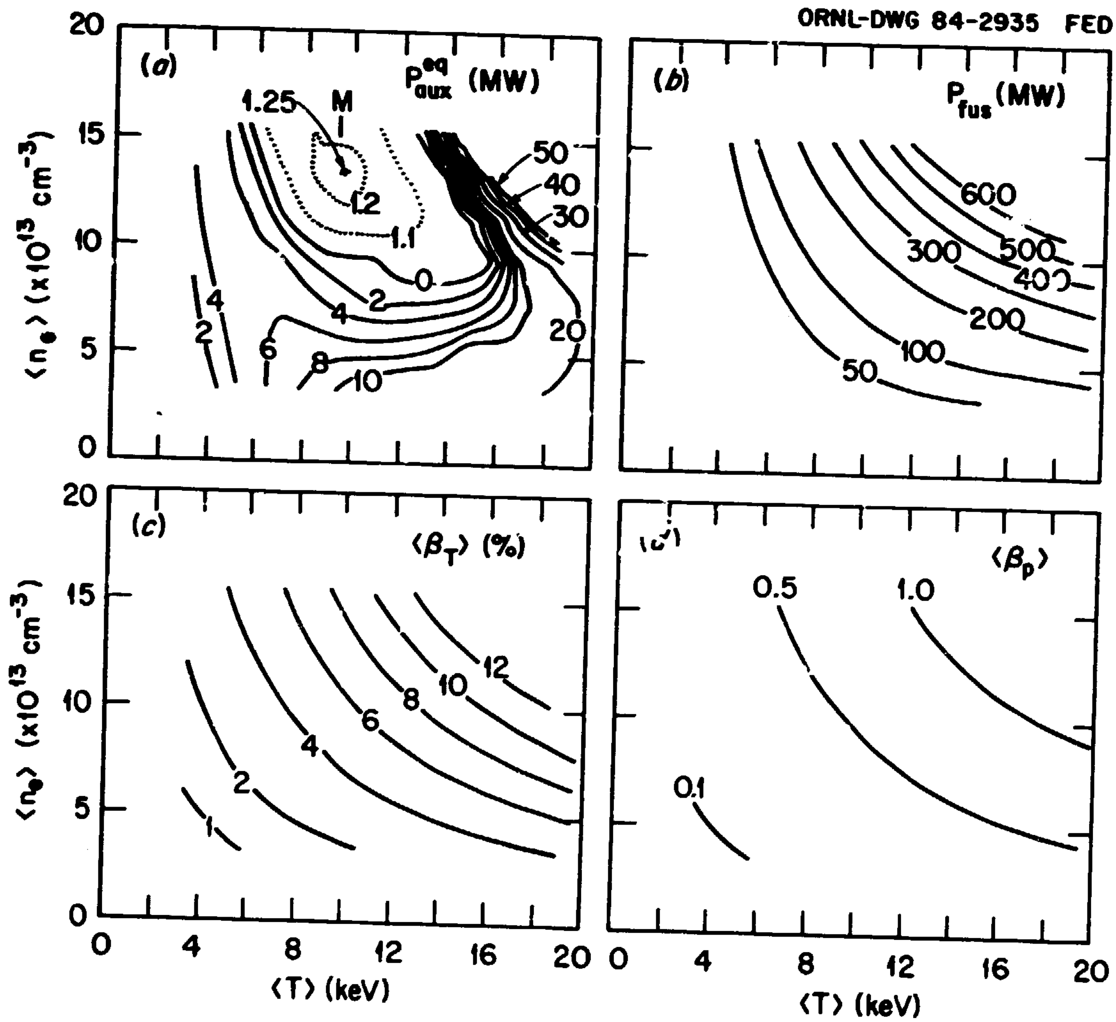

Fig. 8. POPCONs assuming $\chi_{NA} + 0.72\chi_{GMS} \times f(\beta/1.33\beta_c)$ and $n_{ox} = 6 \times 10^{11}$ cm^{-3}.

3.2 SENSITIVITY OF RESULTS

Several modeling parameters introduce variability in these results, although the qualitative features of the POPCONs are as shown above. A somewhat different device [with R_0 = 3.75 m, a = 1.07 m, κ = 1.6, δ = 0.3, B_0 = 4.3 T, and q(a) = 2] was chosen for these studies assuming GMS scaling with sawtoothing; the results are representative. The fractional change in the minimum ignition density (Δ) is the most important result. When the sawtoothing period τ_{ST} is varied, the change is $\Delta(\tau_{ST}$ = 0.75 s) = +8% and $\Delta(\tau_{ST}$ = 0.1 s) = -5%. If sawtoothing is triggered instead by q(0), then, in going from q(0) = 0.98 to q(0) = 0.999, the change is $\Delta \lesssim$ 1%. Quasi-static performance during sawtoothing has been obtained by time averaging the various plasma quantities over each sawtooth period. The parameters associated with the best (worst) confinement are also obtained corresponding to the lowest (highest) auxiliary power during each sawtooth. An ignition contour based on this maximum (minimum) auxiliary power has Δ = +33% (-9%). For the larger device discussed in Sect. 3.1, this variation is Δ = ±10%. This sensitivity indicates the importance of using time-averaged values for quasi-static performance. The feedback time (800 ms) for the auxiliary heating response was chosen to be longer than the sawtooth period (400 ms) but shorter than an energy confinement time (>1 s). A shorter feedback time (400 ms) yields bumpier contours, indicating the importance of proper feedback time. Thus, the quasi-static POPCON analysis is relatively insensitive to details of the sawtoothing transients but sensitive to experimental parameters like feedback time and plasma size. The Δ value is -8% when the Gaussian width of the ICRH-like deposition is narrowed from r_0/a = 0.5 to 0.3, and Δ = 2% if r_0/a is broadened from 0.5 to 0.6. The narrow ICRH deposition is spread over the entire sawtoothing region, yielding performance that is insensitive to the Gaussian width. There is very little sensitivity to the fraction of rf power to the ions (f_i) and electrons (f_e) because the fusion power is completely dominant at ignition. However, the power to surmount the saddle point in P_{aux}^{eq} is 33% lower for f_i/f_e = 100/0 than for f_i/f_e = 75/25 due to the hotter ions below ignition. This simple rf model seems adequate; sophisticated

ICRH modeling of mode conversion and ray tracing may not be needed in the presence of sawtoothing. Raising q(a) to 2.5 yields Δ = 23% because χ^{GMS} increases [$\propto$ q(a)] faster than the effective decrease in transport due to the smaller sawtoothing region. The value of minimum ignition density rises rapidly for an edge ripple, $\delta(a) > 1.8\%$; when $\delta(a) > 3\%$, more than 100 MW is needed to reach ignition, which lies well above 1.6×10^{14} cm^{-3}. Therefore, the plasma performance modeling is insensitive to the details of sawtoothing and ICRH; edge ripple and q(a) have an important impact.

4. RESULTS FOR JET

The plasma performance of JET has also been examined for both a base case and a smaller bore plasma.

Parameter	Base	Smaller
R_o (m)	2.96	2.71
a (m)	1.25	1.00
κ	1.6	1.6
δ	0.3	0.3
B_o (T)	3.45	3.77

These simulations assume a high-current (7-MA) plasma, making the results optimistic. The nominal current is ≲5 MA. Without sawtoothing, GMS scaling yields optimistic ignition contours for both the basic (curve 1 of Fig. 9) and small-bore JET (curve 2). With sawtoothing (curves 3 and 4 in Fig. 9), ignition is less optimistic but attainable. A soft-β modification[14] can be made to GMS scaling of the form

$$\chi_e = \chi^{GMS} \times 0.5 \exp(\varepsilon\beta_p/0.4) ,$$

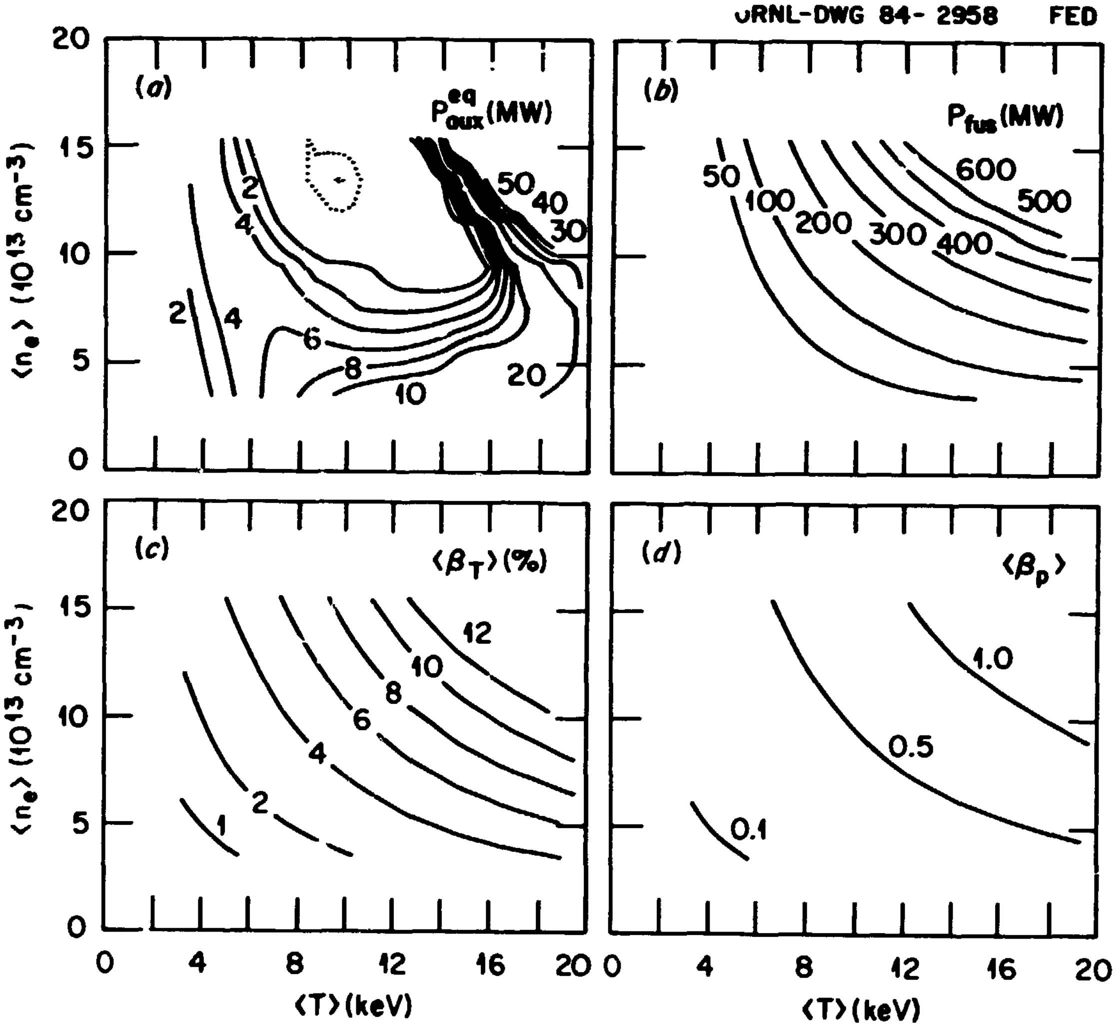

Fig. 9. Ignition contours for JET (see text).

to fit present experiments without sawtoothing. Curve 5 in Fig. 9 is the resulting ignition contour for the basic JET; the smaller-bore JET has no corresponding ignition curve for $n_e < 2 \times 10^{14}$ cm^{-3}. The associated plasma parameters for the minimum-density ignition points are summarized in Table 1. JET appears ignitable using transport assumptions similar to TFCX.

Table 1. Ignition parameters for JET

Curve	Sawtoothing	n_e (10^{14} cm^{-3})	T (keV)	β_T (%)	β_p	P_{fus} (MW)
1	No	0.51	9.0	3.8	0.28	50
2 (small)	No	0.63	9.5	4.0	0.28	40
3	Yes	0.52	17.1	7.9	1.05	130
4 (small)	Yes	0.67	19.0	9.7	0.90	150
5 (soft beta)	No	1.45	12.3	15.0	3.20	530

5. PERFORMANCE SUMMARY

TFCX appears ignitable with sawtoothing and a reasonable range of electron thermal diffusivity scalings. Transport simulations show that $\lesssim$25 MW of ICRH is adequate for heating in TFCX. Ignition appears inaccessible if $\chi_e = 2 \times \chi^{GMS}$ with sawtoothing, but performance at the nominal burn point would be unchanged. The model is insensitive to the details of sawtoothing transients and ICRH deposition. Edge ripple and q(a) have a large impact. For optimistically high currents, JET appears ignitable using transport scalings similar to TFCX.

ACKNOWLEDGMENT

The numerous and insightful suggestions by S. E. Attenberger (CTD/ORNL) are gratefully acknowledged.

REFERENCES

1. W. A. Houlberg, S. E. Attenberger, and L. M. Hively, "Contour Analysis of Fusion Reactor Plasma Performance," Nucl. Fusion 22, 935 (1982).
2. L. L. Lao, "VMOMS — A Computer Code for Finding Moment Solutions to the Grad-Shafranov Equation," Comput. Phys. Commun. 27, 129 (1982).
3. L. L. Lao, S. P. Hirshman, and R. M. Wieland, "Variational Moment Solutions to the Grad-Shafranov Equation," Phys. Fluids 24, 1431 (1981).
4. D. E. Post et al., "Steady State Radiative Cooling Rates for Low-Density, High-Temperature Plasmas," At. Data Nucl. Data Tables 20, 397 (1977).
5. D. R. Mikkelsen, Princeton Plasma Physics Laboratory, personal communication, September 1983.
6. W. Pfeiffer, "Energy Transport Due to Sawtooth Oscillations in the Doublet III Tokamak," GA-A16959, GA Technologies, Inc., February 1983.
7. F. L. Hinton and R. D. Hazeltine, "Theory of Plasma Transport in Toroidal Confinement Systems," Rev. Mod. Phys. 48, 239 (1976).
8. R. J. Hastie and W. N. G. Hitchon, "Energy Loss Due to Ripple Effects in INTOR," in *European Contribution to the Third Workshop Meeting*, Phase IIa, December 1981.
9. E. Apgar et al., "High-Density and Collisional Plasma Regions in the Alcator Programme," in *Proceedings of the Sixth International Conference on Plasma Physics and Controlled Nuclear Fusion Research*, vol. 1, IAEA, Vienna, 1977, p. 247.
10. E. P. Gorbunov, S. V. Mirnov, and V. S. Strelkov, "Energy Confinement Time of a Plasma as a Function of the Discharge Parameters in Tokamak-3," Nucl. Fusion 10, 43 (1970).
11. A. Sykes et al., "Beta Limits in Tokamaks due to High-n Ballooning Modes," in *Proceedings of the Eleventh European Conference on Controlled Fusion and Plasma Physics, Aachen, 1983*, vol. 7D, Part II, 1983, p. 363.

12. J. A. Schmidt, "The Toroidal Fusion Core Experiment Studies," paper IAEA-CN-44/U-I-3 presented at the Tenth International Conference on Plasma Physics and Controlled Nuclear Fusion Research, London, September 12-19, 1984; to be published in the proceedings.

13. L. C. Bernard et al., "MHD Beta Limits: Scaling Laws and Comparison with Doublet III Data," Nucl. Fusion 23, 1475 (1983).

14. J. Sheffield, Oak Ridge National Laboratory, personal communication, October 1983.

ORNL/FEDC-84/1
Dist. Category UC-20 c,d

INTERNAL DISTRIBUTION

1. S. E. Attenberger
2. L. A. Berry
3. R. J. Colchin
4. R. A. Dory
5. J. L. Dunlap
6. G. E. Gorker
7. J. R. Haines
8. W. D. Nelson
9. M. J. Saltmarsh
10. J. Sheffield
11. D. J. Sigmar
12. V. C. Srivastava
13. Y-K. M. Peng
14–18. L. M. Hively
19. D. R. Baumgardner
20–21. Laboratory Records Department
22. Laboratory Records, ORNL-RC
23. Central Research Library
24. Document Reference Section
25. ORNL Patent Office
26. Fusion Energy Division Library
27. Fusion Energy Division Publications Office

EXTERNAL DISTRIBUTION

28–32. D. R. Mikkelsen, Princeton Plasma Physics Laboratory, P.O. Box 451, Princeton, NJ 08544
33. M. A. Abdou, School of Engineering and Applied Science, 6288 Boelter Hall, University of California, Los Angeles, CA 90024
34. C. A. Anderson, Westinghouse Electric Corporation, Advanced Energy Systems Division, P.O. Box 158, Madison, PA 15663
35. J. L. Anderson, CMB-3, Mail Stop 348, Los Alamos National Laboratory, P.O. Box 1663, Los Alamos, NM 87545
36. C. C. Baker, FPP/208, Argonne National Laboratory, 9700 South Cass Avenue, Argonne, IL 60439
37. D. S. Beard, Office of Fusion Energy, Office of Energy Research, Mail Stop G-256, U.S. Department of Energy, Washington, DC 20545
38. K. L. Black, Department E452, McDonnell Douglas Astronautics Company, P.O. Box 516, St. Louis, MO 63166
39. R. Botwin, C47-05, Grumman Aerospace Corporation, P.O. Box 31, Bethpage, NY 11714
40. W. B. Briggs, McDonnell Douglas Astronautics Company, P.O. Box 516, St. Louis, MO 63166
41. J. N. Brooks, FPP/207, Argonne National Laboratory, 9700 South Cass Avenue, Argonne, IL 60439
42. S. C. Burnett, GA Technologies, Inc., P.O. Box 81608, San Diego, CA 92138
43. J. D. Callen, Department of Nuclear Engineering, University of Wisconsin, Madison, WI 53706
44. D. R. Cohn, MIT Plasma Fusion Center, 167 Albany Street, Cambridge, MA 02139
45. J. W. Coursen, C36-05, Grumman Aerospace Corporation, P.O. Box 31, Bethpage, NY 11714
46. R. W. Conn, School of Chemical, Nuclear, and Thermal Engineering, Boelter Hall, University of California, Los Angeles, CA 90024

47. J. G. Crocker, EG&G Idaho, P.O. Box 1625, Idaho Falls, ID 83401
48. G. R. Dalton, Department of Nuclear Engineering Science, Nuclear Science Center, University of Florida, Gainesville, FL 32611
49. R. C. Davidson, Massachusetts Institute of Technology, 77 Massachusetts Avenue, Cambridge, MA 02139
50. N. A. Davies, Office of Fusion Energy, Office of Energy Research, Mail Station G-256, U.S. Department of Energy, Washington, DC 20545
51. S. O. Dean, Director, Fusion Energy Development, Science Applications, Inc., 2 Professional Drive, Suite 249, Gaithersburg, MD 20760
52. J. F. Decker, Office of Fusion Energy, Office of Energy Research, Mail Stop G-256, U.S. Department of Energy, Washington, DC 20545
53. D. DeFreece, E451, Building 81/1/B7, McDonnell Douglas Astronautics Company, P.O. Box 516, St. Louis, MO 63166
54. J. N. Doggett, L-441, Lawrence Livermore National Laboratory, P.O. Box 808, Livermore, CA 94550
55. H. Dreicer, Division Leader, CRT, Los Alamos National Laboratory, P.O. Box 1663, Los Alamos, NM 87545
56. D. Ehst, Argonne National Laboratory, 9700 South Cass Avenue, Argonne, IL 60439
57. F. Farfaletti-Casali, Engineering Division, Joint Research Center, Ispra Establishment, 21020 Ispra (Varese), Italy
58. P. A. Finn, Fusion Power Program, Argonne National Laboratory, 9700 South Cass Avenue, Argonne, IL 60439
59. H. K. Forsen, Bechtel Group, Inc., Research & Engineering, P.O. Box 3965, San Francisco, CA 94119
60. J. S. Foster, Jr., Building R4-2004, TRW Defense and Space Systems, 1 Space Park, Redondo Beach, CA 90278
61. T. K. Fowler, Associate Director for MFE, L-436, Lawrence Livermore National Laboratory, P.O. Box 808, Livermore, CA 94550
62. J. W. French, EBASCO Services, Inc., Forrestal Campus, CN-59, Princeton University, Princeton, NJ 08544
63. H. P. Furth, Director, Princeton Plasma Physics Laboratory, P.O. Box 451, Princeton, NJ 08544
64. J. G. Gavin, Jr., President, A01-11, Grumman Aerospace Corporation, P.O. Box 31, Bethpage, NY 11714
65. G. Gibson, Westinghouse Electric Corporation, Advanced Energy Systems Division, P.O. Box 158, Madison, PA 15663
66. J. R. Gilleland, Manager, Fusion Project, GA Technologies, Inc., P.O. Box 81608, San Diego, CA 92138
67. M. Y. Gohar, Argonne National Laboratory, 9700 South Cass Avenue, Argonne, IL 60439
68. R. W. Gould, Department of Applied Physics, California Institute of Technology, Pasadena, CA 91109
69. M. W. Griffin, Department E236, McDonnell Douglas Astronautics Company, P.O. Box 516, St. Louis, MO 63166
70. C. R. Head, Office of Fusion Energy, Office of Energy Research, Mail Stop G-256, U.S. Department of Energy, Washington, DC 20545
71. C. D. Henning, Lawrence Livermore National Laboratory, P.O. Box 808, Livermore, CA 94550
72. J. J. Holmes, Westinghouse-Hanford Engineering Development Laboratory, P.O. Box 1970, Richland, WA 99352
73. D. Hwang, Princeton Plasma Physics Laboratory, P.O. Box 451, Princeton, NJ 08544
74. J. B. Joyce, Princeton Plasma Physics Laboratory, P.O. Box 451, Princeton, NJ 08544

75. R. A. Krakowsi, CTR-12, Mail Stop 641, Los Alamos National Laboratory, P.O. Box 1663, Los Alamos, NM 87545
76. G. L. Kulcinski, University of Wisconsin, Department of Nuclear Engineering, Engineering Research Building, Room 439, 1500 Johnson Drive, Madison, WI 53706
77. D. L. Kummer, McDonnell Douglas Astronautics Company, P.O. Box 516, St. Louis, MO 63166
78. W. Marton, Office of Fusion Energy, Office of Energy Research, Mail Station G-256, U.S. Department of Energy, Washington, DC 20545
79. L. G. Masson, EG&G Idaho, Idaho National Engineering Laboratory, P.O. Box 1625, Idaho Falls, ID 83401
80. D. M. Meade, Princeton Plasma Physics Laboratory, P.O. Box 451, Princeton, NJ 08544
81. A. T. Mense, Building 107, Post B2, McDonnell Douglas Astronautics Company, P.O. Box 516, St. Louis, MO 63166
82. R. W. Moir, Lawrence Livermore National Laboratory, P.O. Box 808, Livermore, CA 94550
83. D. B. Montgomery, MIT Plasma Fusion Center, 167 Albany Street, Cambridge, MA 02139
84. A. E. Munier, Grumman Aerospace Company, P.O. Box 31, Bethpage, NY 11714
85. R. E. Nygren, FPP/207, Argonne National Laboratory, 9700 South Cass Avenue, Argonne, IL 60439
86. T. Ohkawa, GA Technologies, Inc., P.O. Box 81608, San Diego, CA 92138
87. J. A. O'Toole, Plasma Physics Laboratory, Building I-P, Room 8A, James Forrestal Campus, P.O. Box 451, Princeton, NJ 08544
88. R. R. Parker, Francis Bitter National Magnet Laboratory, 170 Albany Street, Cambridge, MA 02139
89. B. Pease, Culham Laboratory, Abingdon, Oxfordshire OX14 3DB, United Kingdom
90. M. Pelovitz, Princeton Plasma Physics Laboratory, P.O. Box 451, Princeton, NJ 08544
91. F. W. Perkins, Princeton Plasma Physics Laboratory, P.O. Box 451, Princeton, NJ 08544
92. M. Porkolab, Massachusetts Institute of Technology, 77 Massachusetts Avenue, Cambridge, MA 02139
93. D. E. Post, Princeton Plasma Physics Laboratory, P.O. Box 451, Princeton, NJ 08544
94. L. K. Price, Department of Energy, Oak Ridge Operations, P.O. Box E, Oak Ridge, TN 37831
95. R. E. Price, Office of Fusion Energy, Office of Energy Research, Mail Station G-256, U.S. Department of Energy, Washington, DC 20545
96. F. A. Puhn, GA Technologies, Inc., P.O. Box 81608, San Diego, CA 92138
97. J. Purcell, GA Technologies, Inc., P.O. Box 81608, San Diego, CA 92138
98. R. V. Pyle, University of California, Lawrence Berkeley Laboratory, Berkeley, CA 94720
99. J. M. Rawls, GA Technologies, Inc., P.O. Box 81608, San Diego, CA 92138
100. M. Roberts, Office of Fusion Energy, Office of Energy Research, Mail Stop G-256, U.S. Department of Energy, Washington, DC 20545
101. J. D. Rogers, Los Alamos National Laboratory, P.O. Box 1663, Los Alamos, NM 87545
102. M. L. Rogers, Monsanto Research Corporation, Mound Laboratory Facility, P.O. Box 32, Miamisburg, OH 45342
103. M. N. Rosenbluth, RLM 11.218, Institute for Fusion Studies, University of Texas, Austin, TX 78712
104. P. H. Rutherford, Princeton Plasma Physics Laboratory, P.O. Box 451, Princeton, NJ 08544
105. J. A. Schmidt, Princeton Plasma Physics Laboratory, P.O. Box 451, Princeton, NJ 08544
106. J. Schultz, MIT Plasma Fusion Center, 167 Albany Street, Cambridge, MA 02139
107. F. R. Scott, Electric Power Research Institute, P.O. Box 10412, Palo Alto, CA 94304

108. G. Sheffield, Princeton Plasma Physics Laboratory, P.O. Box 451, Princeton, NJ 08544
109. D. Smith, Materials Science Division, Argonne National Laboratory, 9700 South Cass Avenue, Argonne, IL 60439
110. W. M. Stacey, Jr., Georgia Institute of Technology, School of Nuclear Engineering, Atlanta, GA 30332
111. E. Stern, Grumman Aerospace Corporation, CN-59, Forrestal Campus, Princeton, NJ 08544
112. P. M. Stone, Office of Fusion Energy, Office of Energy Research, Mail Station G-256, U.S. Department of Energy, Washington, DC 20545
113. I. N. Sviatoslavsky, Room 33, Engineering Research Building, 1500 Johnson Drive, University of Wisconsin, Madison, WI 53706
114. R. E. Tatro, Manager, Energy Systems, M.Z. 16-1070, General Dynamics–Convair Division, P.O. Box 80847, San Diego, CA 92138
115. F. Thomas, B-20-5, Grumman Aerospace Corporation, Bethpage, NY 11714
116. K. I. Thomassen, Lawrence Livermore National Laboratory, P.O. Box 808, Livermore, CA 94550
117. R. J. Thome, Francis Bitter National Magnet Laboratory, 170 Albany Street, Cambridge, MA 02139
118. C. Trachsel, McDonnell Douglas Astronautics Company, P.O. Box 516, St. Louis, MO 63166
119. A. W. Trivelpiece, Office of Fusion Energy, Office of Energy Research, Mail Station G-256, U.S. Department of Energy, Washington, DC 20545
120. L. R. Turner, Fusion Power Program, Argonne National Laboratory, 9700 South Cass Avenue, Argonne, IL 60439
121. E. H. Valeo, Princeton Plasma Physics Laboratory, P.O. Box 451, Princeton, NJ 08544
122. K. E. Wakefield, Princeton Plasma Physics Laboratory, P.O. Box 451, Princeton, NJ 08544
123. J. C. Wesley, GA Technologies, Inc., P.O. Box 81608, San Diego, CA 92138
124. H. Willenberg, Mathematical Sciences Northwest, Inc., P.O. Box 1887, Bellevue, WA 98009
125. J. E. C. Williams, Francis Bitter National Magnet Laboratory, 170 Albany Street, Cambridge, MA 02139
126. H. H. Yoshikawa, W/A-62, Hanford Engineering Development Laboratory, P.O. Box 1970, Richland, WA 99352
127. K. M. Young, Princeton Plasma Physics Laboratory, P.O. Box 451, Princeton, NJ 08544
128. N. E. Young, EBASCO Services, Inc., Princeton Plasma Physics Laboratory, P.O. Box 451, Princeton, NJ 08544
129. Bibliothek, Max-Planck-Institut fur Plasmaphysik, D-8046 Garching bei Munchen, Federal Republic of Germany
130. Bibliothek, Institut fur Plasmaphysik, KFA, Postfach 1913, D-5170 Julich, Federal Republic of Germany
131. Library, Centre de Recherches en Physique des Plasmas, 21 Avenue des Bains, 1007 Lausanne, Switzerland
132. Bibliotheque, Service du Confinement des Plasmas, CEA, B.P. No. 6, 92 Fontenay-aux-Roses (Seine), France
133. Documentation S.I.G.N., Department de la Physique du Plasma et de la Fusion Controlee, Association EURATOM-CEA, Centre d'Etudes Nucleaires, B.P. 85, Centre du Tri, 38041 Grenoble, Cedex, France
134. Library, Centre de Recherches en Physique des Plasmas, 21 Avenue des Bains, 1007 Lausanne, Switzerland

135. Library, Culham Laboratory, UKAEA, Abingdon, Oxfordshire, OX14 3DB, England
136. Library, FOM Instituut voor Plasma-Fysica, Rijnhuizen, Jutphaas, Netherlands
137. Library, Institute of Physics, Academia Sinica, Beijing, Peoples Republic of China
138. Library, Institute for Plasma Physics, Nagoya University, Nagoya 464, Japan
139. Library, International Centre for Theoretical Physics, Trieste, Italy
140. Library, JET Joint Undertaking, Abingdon, Oxfordshire, OX14 3I ...nd
141. Library, Laboratorio Gas Ionizzati, Frascati, Italy
142. Plasma Research Laboratory, Australian National Laboratory, P.O. Box 4, Canberra, ACT 2000, Australia
143. Thermonuclear Library, Japan Atomic Energy Research Institute, Tokai, Naka, Ibaraki, Japan
144. Library, Plasma Physics Laboratory, Kyoto University, Gokasho Uji, Kyoto, Japan

145–340. Given distribution as shown in TID-4500, Magnetic Fusion Energy (Category Distribution UC-20 c,d: Reactor Materials and Fusion Systems)

☆U.S. GOVERNMENT PRINTING OFFICE: 1984-544-045/4211